LAWRENCE
LIVERMORE
NATIONAL
LABORATORY

LLNL-CONF-679759

Part damage due to proximity effects during sub-micron additive manufacturing via two-photon lithography

S. Saha, C. Divin, J. Cuadra, R. Panas

December 1, 2015

ASME Manufacturing Science and Engineering Conference 2016
Blacksburg, MA, United States
June 27, 2016 through July 1, 2016

Disclaimer

Proceedings of the 2016 Manufacturing Science and Engineering Conference
MSEC2016
June 27-July 1, 2016, Virginia Tech, Blacksburg, USA

MSEC2016-8793

PART DAMAGE DUE TO PROXIMITY EFFECTS DURING SUB-MICRON ADDITIVE MANUFACTURING VIA TWO-PHOTON LITHOGRAPHY

Sourabh K. Saha[1], Chuck Divin, Jefferson A. Cuadra, Robert M. Panas
Materials Engineering Division
Lawrence Livermore National Laboratory
Livermore, CA, USA
[1]Corresponding author: saha5@llnl.gov

KEYWORDS

Laser damage, two-photon absorption, resist boiling, overlapping features.

ABSTRACT

Two-photon lithography is a direct laser write process that enables fabrication of millimeter scale 3D structures with nanoscale building blocks. In this technique, writing is achieved via a nonlinear two-photon absorption process during which two photons are near-simultaneously absorbed at high laser intensities. Due to the high laser intensities, it is essential to carefully select the incident power so that two-photon polymerization (TPP) occurs without any laser damage of the resist. Currently, the feasible range of laser power is identified by writing small test patterns at varying power levels. Herein, we demonstrate that the results of these tests cannot be generalized because the damage threshold power is dependent on the proximity of features and reduces by as much 37.5% for overlapping features. We have identified that this reduction occurs due to a combination of reduced TPP for overlapping features and increased single-photon absorption of the resin after curing. We have captured the damage arising out of this proximity effect via 3D computed tomography images of a non-homogenous part that has varying feature density. Part damage manifests in the form of internal spherical voids that arise due to boiling of the resist at high laser intensities. Herein, we have empirically quantified this proximity effect by identifying the damage threshold power at different writing speeds and feature overlap spacings. In addition, we present a first-order analytical model that captures the scaling of this proximity effect. The scaling laws and the empirical data generated here can be used to select the appropriate writing process parameters so as to correct for proximity effects and prevent part damage during sub-micron additive manufacturing of parts with closely spaced features.

INTRODUCTION

The absence of well-characterized scalable nanomanufacturing processes that are capable of fabricating macroscale parts with nanometer scale features is a key bottleneck in transitioning several promising nano-enabled devices from the research laboratory to real-world adoption. The two-photon absorption based laser direct write process is a viable candidate for scalable nanomanufacturing as it enables fabrication of millimeter scale parts with sub-micron building blocks. This is achieved by a combination of the ability to (i) cure a sub-micron volume around the focal spot in the resist via two-photon polymerization (TPP) [1,2], (ii) scan the focal spot via high speed galvanometers [3-5], and (iii) stitch together several micro-scale printed sections. As such, two-photon polymerization is a promising technique for additive manufacturing of 3D structures with sub-micron features. However, this process is currently of limited practical import for additive manufacturing due to the inability to predictively fabricate high-quality parts that satisfy the desired tolerances. Currently, part quality is achieved via a series of expensive and time consuming empirical trial-and-error parameter selection procedures. Herein, we demonstrate that such empirical guide-rules cannot be successfully generalized over a broad operating region. Specifically, we demonstrate the presence of laser damage due to proximity effects. To overcome this limitation, we present a first-order model to predict the change in this proximity effect with process parameters.

The two-photon absorption phenomenon can be used to initiate the same molecular transition in the photoinitiator as that initiated by a single-photon absorption process but at twice the wavelength [6]. This is possible due to the near-simultaneous absorption of two photons before the initiation of the molecular transition. Two-photon absorption is fundamentally different from the more commonly observed

single-photon absorption. During single-photon absorption, the rate of molecular transition is linearly dependent on light intensity. For example, the power density absorbed by the resist during UV lithography is linearly related to the UV light intensity. In contrast, the rate of molecular transition during two-photon absorption has a quadratic dependence on the laser intensity. Additionally, two-photon absorption is several orders of magnitude weaker than single-photon absorption. Therefore, it is possible to spatially restrict the two-photon absorption process to a sub-diffraction volume by focusing a high-intensity laser to a diffraction-limited spot. To ensure that the focused spot is polymerized only via two-photon absorption, the resist is carefully selected to be nominally non-absorbing at the single-photon wavelength. This is commonly achieved by selecting near-IR pulsed lasers to illuminate UV resists. Such resists are nominally non-absorbing at IR while being photo-active at half wavelength. Thus, this scheme enables using commonly available UV resists for two-photon polymerization.

Laser damage occurs during TPP when the incident intensity is higher than that required for polymerization of the resist [7]. Laser damage results in the formation of bubbles in the resist that hinder further printing and weaken the printed structure. Thus, during printing one must ensure that the laser power and writing speed are properly selected to lie below the damage threshold. This is commonly achieved by running a series of empirical tests wherein a set of small calibration structures are fabricated at increasing laser powers and speeds. Although such empirical tests can provide valuable estimates for the threshold, they are ineffective to predict the damage threshold over a wide operating regime. For example, we have observed that the damage threshold varies over a wide range with changes in the feature density, i.e., the damage threshold is dependent on the proximity of the features. Additionally, this proximity effect varies with the writing speed. This behavior arises due to the changes in the absorption spectrum of the resist during the curing process. The absorptivity of the polymerized resin at the incident IR wavelength increases to a non-negligible value post curing. Herein, we have captured the effect of this additional absorption mode in terms of the proximity effect for laser damage.

Proximity effects reduce the laser damage threshold and make a feature-dense part susceptible to defects. Herein, we have recorded these defects arising out of proximity effects by capturing 3D computed tomography images of internal voids/bubbles that were generated via boiling of the resist during printing of the part. We have quantified this proximity effect by tracking the effect of feature spacing on the damage threshold power. Finally, we have developed an analytical model to predict the proximity effect arising out of the additional IR absorption by the cured resin. This analytical model may be used to identify the safe operating parameters during TPP to predictively fabricate high-quality 3D parts.

DEMONSTRATION OF PROXIMITY EFFECT

We have observed the significant role of proximity effects in reducing the laser damage threshold power by recording 3D computed tomography (CT) images of a non-homogenous printed part. The phase contrast CT image of the part and a CAD model of the part are shown in Fig. 1. The defects are visible in the form of internal voids in the CT images that arise due to boiling of the resist at the feature-dense cavity walls. Such internal voids are not visible via surface imaging techniques such as scanning electron microscopy. However, these internal voids adversely affect the quality of the part and must be eliminated when a high part quality is desired.

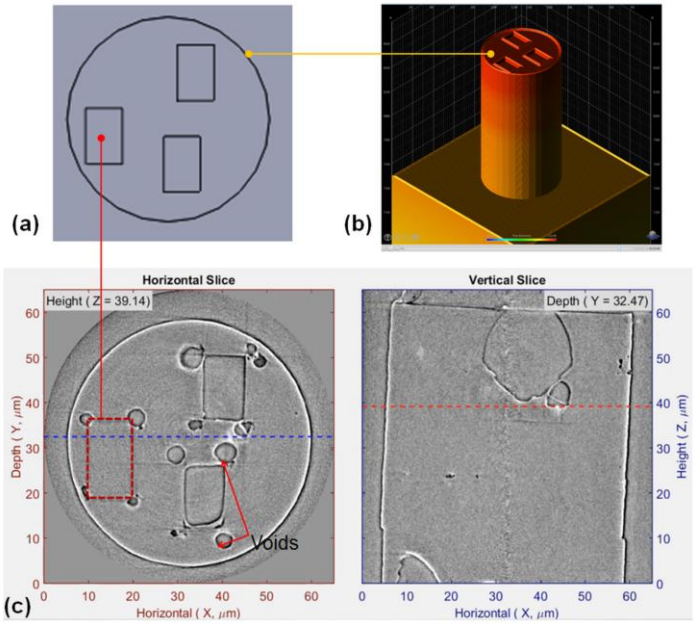

Fig. 1: Designed versus fabricated part with internal cavities. (a) Lateral cross-section of the designed part. (b) Discretized model of the part for 3D printing illustrating the part build up to the level of the designed cavities. (c) Phase contrast computed tomography (CT) X-ray image of the fabricated part. The dark-bright edge pairs in the image represent the physical edges between the void space and the cured resin.

3D part fabrication

We have printed the part on a commercially available Nanoscribe GT laser lithography system that implements a TPP based 3D writing technique via Z-piezo scanner and high-speed X-Y galvo scanners. Printing was performed with a proprietary negative tone resist (IP-Dip) that is available from Nanoscribe. The printed part consists of three sets of cavities within a right circular cylinder. The cylinder was 125 um tall and had a designed diameter of 55 um. For ease of material handling during CT imaging, the cylinder was built on top of a large 750 um tall pillar that has a square cross-section of side 125 um. In the cylindrical section, each set of cavities lies on a different horizontal plane and comprises three types of cavities: flat topped, concave topped, and convex topped cavities.

For 3D printing, the part was discretized and printed layer-by-layer wherein each Z layer was spaced by 0.6 um. A log-pile structure was generated with a line spacing of 0.4 um by laying lines along the X axis and then along Y axis in alternate layers. This in-plane spacing was reduced to 0.25 um over an in-plane distance of 2 um at each of the cavity walls and the external wall. The design intent of this high-density wall was to provide a higher wall strength and stiffness to prevent cavity and part collapse. Printing was performed at a linear writing speed of 20 mm/s and an average laser power of 30 mW. These parameters were selected by first writing a small test structure to ensure the absence of laser damage. The absence of laser damage was also verified during printing of the first few layers that had a homogenous in-plane spacing of 0.4 um. However, laser damage was observed in the layers with the dense cavity walls; this damage is evident from the CT images in Fig. 1. This suggests that the laser damage arises due to the proximity effect during printing of the feature-dense cavity walls.

3D part imaging

CT imaging of the printed part was performed on the commercially available Zeiss Xradia UltraXRM-L200 system. This system has an 8 keV X-ray source and utilizes X-ray diffractive optics to image the part. The 3D image was computationally reconstructed from several 2D projection images. These 2D projections were taken by rotating the part relative to a stationary source and detector. A total of 721 projections were collected over a range of 180^0 with each projection lasting for 2 minutes. To correct for system drift during image acquisition, the part was marked with a 2 um gold microsphere, which was tracked using a semi-automated approach. Projections were registered using the drift tracking and reconstructed using in-house tomography software Livermore Tomography Tools (LTT). The field of view was 65 um with a resolution of 0.3 um. Thus, only about the top 60 um of the part is visible in the CT image (Fig. 1c).

CT imaging was performed in the phase contrast mode. Thus, the gray scale image represents the phase shift of the X-ray beam as it passes through the material. The phase contrast mode was selected instead of the more conventional transmission mode due to the low atomic number of the components of the acrylate based resist. Distinct features in the CT images can be identified by identifying the feature edges that comprise a pair of adjacent bright and dark edges. The side with the bright edge corresponds to the cured material whereas the side with the dark edge corresponds to the air medium. Thus, the spherical features in Fig. 1c correspond to pockets of voids that were formed when the resist cured around the bubbles of uncured resist; voids were formed when the part was chemically developed to remove the uncured resist.

QUANTIFICATION OF PROXIMITY EFFECT

Laser damage occurs when the energy absorbed by the resist exceeds the energy required for photo-polymerization. This could occur either when the laser power is too high or when the writing speed is too low. Thus, the damage threshold power must be characterized for a specific writing speed. The effect of writing speed on the quality of features is illustrated in Fig. 2. Laser damage is observed at very low writing speeds whereas no writing is observed at very high writing speed. In addition, the line width reduces with an increase in the writing speed.

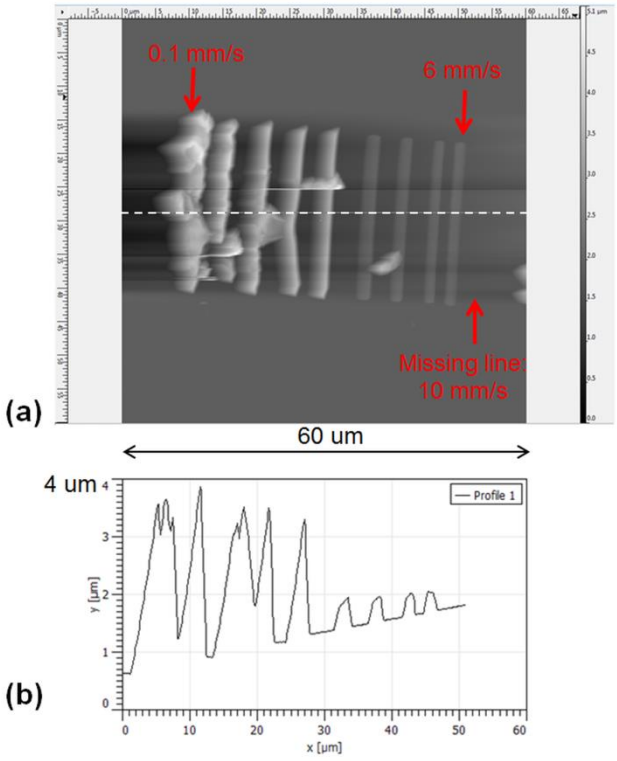

Fig. 2: (a) Atomic force microscope (AFM) image of a set of individual lines written at different laser writing speeds. (b) Profile of the features along the dotted line in the AFM image. Each line was written by moving the laser focal spot across the surface at a uniform velocity and at an average laser power of 25 mW.

Damage threshold for widely spaced lines

The laser damage threshold power at a particular writing speed is the laser power at and above which damage in the part is guaranteed. We have evaluated this threshold power by recording the generation and growth of bubbles during printing of the features. To quantify the damage threshold for widely spaced lines, we have written lines separated by 10 um and at varying laser power levels. During printing, we have recorded the power level at which bubbles were observed. The bubbles were observed in the real-time live images of the printing process as captured via a video camera. Representative images of bubble formation are provided in Fig. 3. The undamaged lines can be identified from the optical images as those lines that are continuous without any breaks whereas the damaged

lines are either discontinuous or have permanent solidified bubble features.

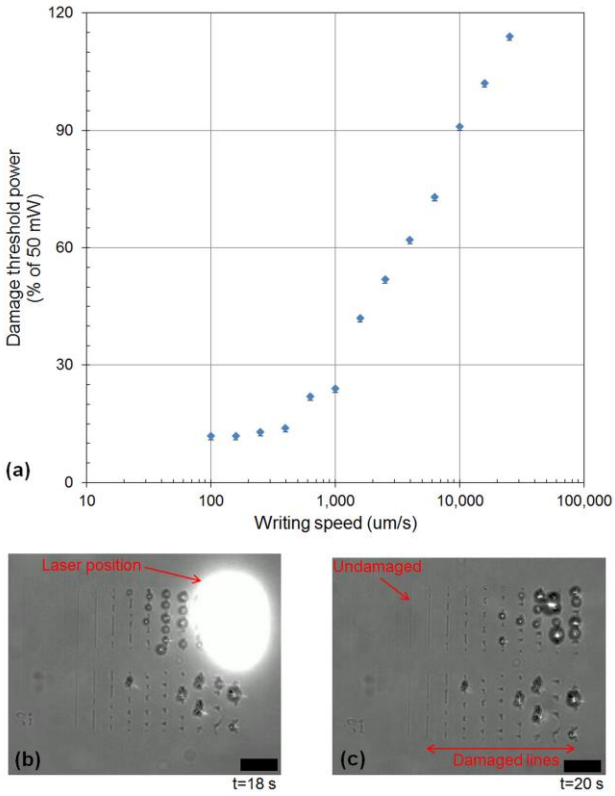

Fig. 3: Damage threshold power during writing of widely spaced individual lines. (a) Effect of writing speed on the damage threshold. (b) Optical image of the writing process illustrating formation of bubbles at high laser power. (c) Optical image of the same region immediately after writing. Damaged lines were identified by the presence of bubbles or discontinuity in the lines. Lines from left to right were written at the same speed but at progressively higher power. Scale bars are 20 um long.

An accurate damage threshold was evaluated by performing these tests in two iterations. In the first iteration, a set of 10 lines was written at the same writing speed but with laser power level progressively increasing by 5 mW across each line starting from the 5 mW level. Data from this test identifies the threshold within 5 mW of the actual value. In the second iteration, another set of 10 lines were written within the 5 mW range identified in iteration 1. The laser power level was varied by 0.5 mW across each line in iteration 2. The data from the second set accurately identifies the threshold within 0.5 mW of the actual value. The results of the second iteration for different writing speeds are summarized in Fig. 3a. The damage threshold power varies from 6 mW at a writing speed of 0.1 mm/s to 57 mW at 25 mm/s. As expected, the damage threshold power increases with the writing speed; this is because the net energy absorbed by a particular material point decreases with an increase in the writing speed. No laser damage is expected during writing of widely spaced lines when the laser power level is chosen to be below this damage threshold. Damage threshold power for speeds higher than 25 mm/s were not observable as the damage threshold for such speeds was higher than the maximum system power of 60 mW.

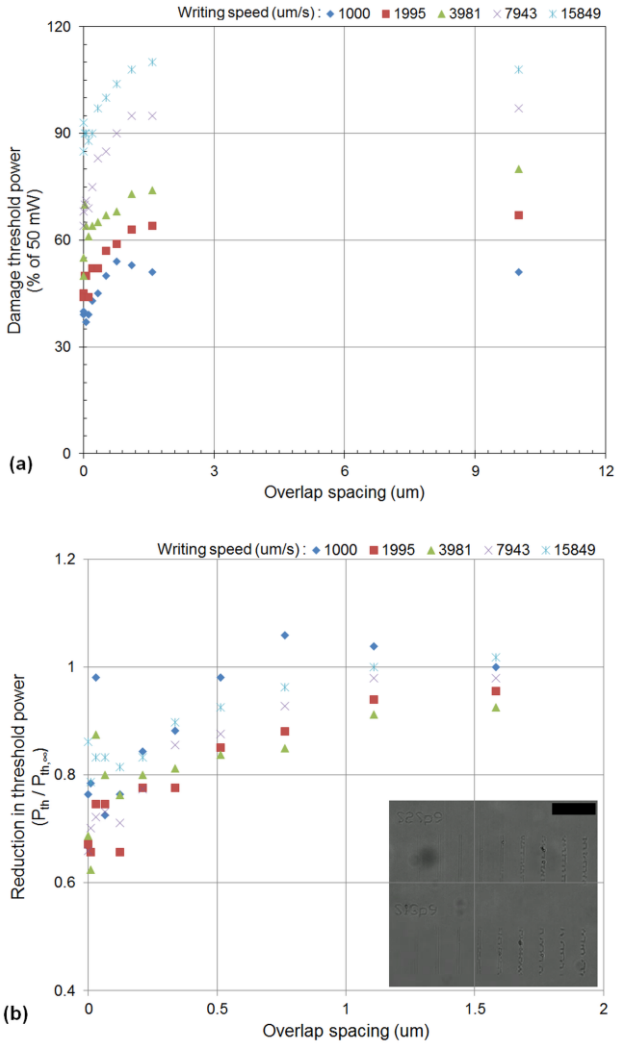

Fig 4: Effect of proximity of writing on the damage threshold power. (a) Damage threshold power versus overlap spacing for two closely spaced lines. (b) The threshold power data from (a) represented as a fraction of the threshold power for widely spaced individual line. Inset is an optical image of the written pattern that comprises pairs of overlapping lines that are separated by 10 um. Scale bar is 20 um long.

Proximity effects

To quantify the proximity effect, we have empirically evaluated the laser damage threshold power during writing of a pair of overlapping lines. Several pairs of overlapping lines were written at different overlap spacings. The same two-step iteration technique was used to accurately identify the damage threshold within 0.5 mW of the actual value. The effect of overlap spacing on the damage threshold is summarized in Fig. 4. The proximity effect is evident from the reduction in damage

threshold while writing closely spaced overlapping lines. The damage threshold reduces by as much as 37.5% during writing of overlapping lines as compared to writing of widely spaced lines. Such overlap line writing is necessary during writing of dense features. Thus, during writing of dense parts, the laser power and writing speed must be carefully selected so that the damage threshold is not exceeded for any feature in the part.

There are two possible sources for the observed proximity effect behavior. First, during writing of overlapping features the energy required for two-photon polymerization of the subsequent line is lower due to the already polymerized volume. Thus, the excess energy is converted into heat and causes laser damage. Second, the absorbed energy is higher because the polymerized and cured resin absorbs single-photon IR radiation. The hypothesis of change in IR absorptivity of the resist after curing is supported by the optical images in Figs. 3 and 4 wherein the printed lines become opaque whereas the surrounding resist medium is transparent to red light. Thus, the resulting proximity effect arises due the combination of both of these absorption modes.

MODELING OF PROXIMITY EFFECT

To explain the proximity effect behavior we have developed a first-order analytical model that captures the essential physics of the damage process in terms of scaling laws for the proximity effect. Fundamentally, laser damage due to boiling of resist occurs when the energy delivered to the resist during laser writing exceeds the energy required for boiling. The transfer of energy from the laser to the resist is determined by laser-matter interactions and the subsequent spatiotemporal distribution of this energy in the resist is determined by heat flow conditions in the resist. As it is not possible to generate a closed-form analytical model that fully captures these physical phenomena, we have made several simplifying approximations. Although these approximations do not capture the full complexity of these phenomena, they are sufficiently accurate to elucidate the scaling of the damage threshold proximity effect during writing of overlapping features.

Absorption from laser

Power absorption

The energy absorbed by the resist can be evaluated from the classical Beer-Lambert absorption relationship. For single-photon absorption, the power density absorbed by the resist is given by:

$$-\frac{\partial I(r,z)}{\partial z} = \alpha I \tag{1}$$

Here, 'I' is the intensity of the laser beam at the radial position 'r' from the beam axis and at an axial distance 'z' within the material. The material property parameter 'α' is the single-photon absorptivity of the material and is dependent on the wavelength of the laser. This absorptivity is nominally zero for the uncured resin and non-zero for the cured resin at the incident laser wavelength of 780 nm.

The power density absorbed by the resist during two-photon absorption is given by a modified absorption relationship as [8]:

$$-\frac{\partial I(r,z)}{\partial z} = \beta I^2 \tag{2}$$

Here, the material property parameter 'β' is the two-photon absorptivity of the material and is dependent on the concentration of the photoinitiator, type of the photoinitiator, and the wavelength of the laser.

Energy absorption

The absorption relationships given by Eqs. (1) and (2) provide the instantaneous power density absorbed by the medium. For damage analysis, one must account for the accumulation of energy over a period of time. For a stationary laser beam, this evaluation is trivial and involves recording the power and duration of exposure. To perform this evaluation for our writing conditions wherein the laser spot is continuously scanned on the surface, we have made the following approximations: (i) the laser spot is stationary throughout the duration of a single pulse and (ii) the laser spot moves discretely with a step size that is equal to the beam width and at such a regular interval that maintains the average writing speed. Out of these two, the first approximation accurately represents the physical condition when ultra-short pulsed lasers are used. In our system, with a writing speed of 25 mm/s, the spot moves by 2.5 femtometer throughout the duration of a pulse that lasts ~100 fs and can be considered stationary. The second approximation leads to an upper bound for the delivered energy and provides a conservative estimate for the damage threshold. Thus, these two approximations transform the line writing condition into a quasi-static dot writing condition. Based on these approximations, the absorbed energy density (U) is evaluated as:

$$U(r,z) = \left(\alpha I + \beta I^2\right)\frac{t_p f_p \sigma}{v} \tag{3}$$

Here, t_p is the duration of a single pulse, f_p is the pulse frequency, v is the laser scan speed, and σ is the beam radius at the axial position z away from the focal plane.

For a Gaussian laser beam, the beam intensity (I) is given by:

$$I(r,z) = \frac{2P}{\pi\sigma^2}\exp\left(-\frac{2r^2}{\sigma^2(z)}\right) \tag{4}$$

Here, P is the transmitted power of each pulse. Thus, the area-averaged energy density for a combination of single-photon and two-photon absorption is given by:

$$\overline{U} = \left(\frac{t_p f_p \sigma_o}{v}\right)\left(0.86\alpha\left(\frac{2P}{\pi\sigma_o{}^2}\right) + 0.98\beta\left(\frac{2P}{\pi\sigma_o{}^2}\right)^2\right) \qquad (5)$$

Here, σ_o is the beam width at the focal plane and the area-averaging is performed over the beam cross-section at the focal plane.

Damage threshold

The damage threshold can be evaluated by comparing the absorbed energy density to the energy density required for polymerization and boiling of the resist at the focal plane. Thus, the damage threshold is determined by the inequality:

$$\overline{U} > \rho h + \left(\frac{w}{2\sigma_o}\right)U_a \qquad (6)$$

Here, ρ is the mass density of the resist, h is the equivalent heat of vaporization of the resist (in J/m^3), i.e., it is the sum of the heat of vaporization and the heat required to raise the temperature of the resist to its boiling point. The energy density U_a is the activation energy required for the polymerization process. The damage threshold condition represented by the inequality (6) is based on the approximation that all of the absorbed energy is confined to the exposed region and leads to a convenient lower bound estimate of the damage threshold power.

For single widely-spaced lines, the single-photon absorptivity of the resist is zero. Thus, the damage threshold power ($P_{th,\infty}$) can be evaluated as:

$$P_{th,\infty} = \left(\frac{\pi^2\sigma_o{}^3\left(\rho h + w/2\sigma_o U_a\right)v}{3.93\beta t_p f_p}\right)^{0.5} \qquad (7)$$

Thus, the threshold power increases with the writing speed and depends on $\sqrt{v}$. This threshold power versus writing speed scaling is supported by the empirical data illustrated in Fig. 3a wherein the least-square fit to power-law dependence yields an exponent of 0.47.

Proximity effect

Writing of closely spaced overlapping features (Fig. 5) differs from writing of widely spaced features in two aspects: (i) a larger fraction of the incident power is absorbed by the resist due to single-photon absorption of the cured resist and (ii) a smaller fraction of the absorbed energy is consumed during the polymerization process due to the preexistence of cured material. In combination, these two factors reduce the laser damage power threshold.

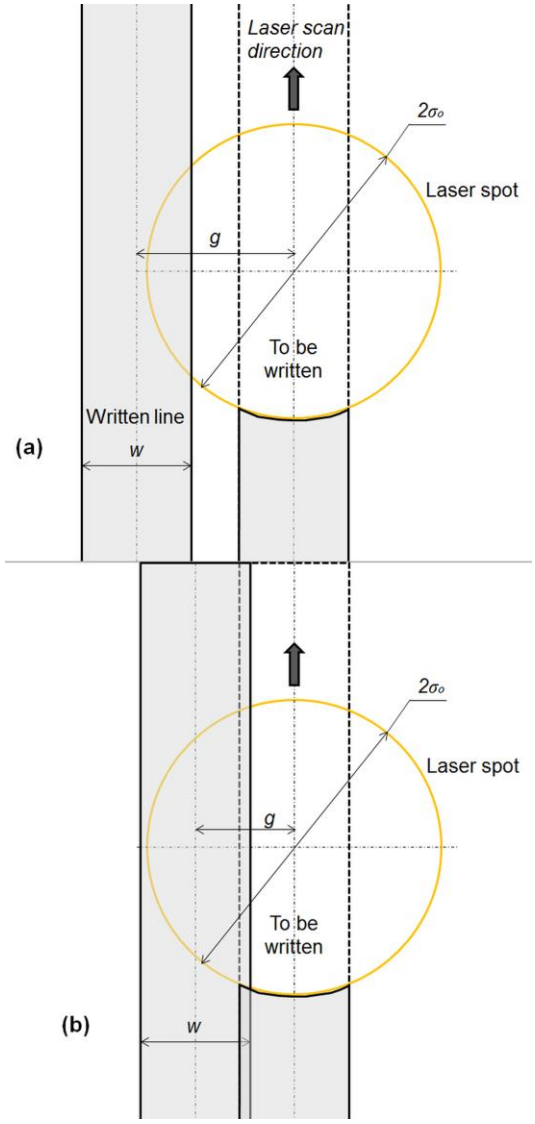

Fig. 5: Location of the pair of closely spaced lines with respect to the laser spot. (a) When the lines do not physically overlap. (b) When the lines physically overlap.

Reduced TPP

When the overlap spacing between successive lines (g) is less than the line width (w), there is preexisting cured material in the exposed region that does not consume activation energy for polymerization. Thus, during writing of a pair of lines, the effective activation energy for the second line can be estimated as:

$$U_{a,eff} \sim \frac{g}{w}U_a \qquad (8)$$

This reduces the damage threshold power due to reduced TPP ($P_{th,T}$) as:

$$\frac{P_{th,T}}{P_{th,\infty}} = \left(\frac{\rho h + (0.5g/\sigma_o)U_a}{\rho h + (0.5w/\sigma_o)U_a} \right)^{0.5} \quad (9)$$

One may deduce from Eq. (9) that: (i) the damage threshold ratio ($P_{th,T}/P_{th,\infty}$) does not depend on the writing speed and (ii) the damage threshold would not change with further increase in the overlap spacing when the overlap spacing exceeds the line width. Both of these model deductions are inconsistent with the empirical data summarized in Fig. 4. To reconcile this discrepancy, an additional laser absorption mode based on the single-photon absorption by the cured resin must be accounted for.

Increased single-photon absorption

Here, we have modeled the increased single-photon absorption by introducing an effective non-zero single-photon absorptivity (α_{eff}) for the resist. This absorptivity can be estimated as an area-averaged absorptivity wherein the cured resin has non-zero absorptivity (α) and the uncured resin has zero absorptivity. Thus, the effective absorptivity is given by:

$$\alpha_{eff} \sim \left(\frac{\sigma_o + 0.5w - g}{\sigma_o + 0.5w} \right) \left(\frac{w}{\sigma_o} \right) \alpha \quad (10)$$

This non-zero effective absorptivity exists only for the case when the overlap spacing g lies in the range of (σ_o-0.5w) < g < (σ_o+0.5w). Above this limit, the adjacent feature lies outside the laser beam and does not influence nearby features. Below this limit, the entire feature is within the beam such that $\alpha_{eff} \sim (w/\sigma_o)\alpha$. The reduced damage threshold due to the combined effect ($P_{th,C}$) in this range is then given by:

$$\left(\frac{P_{th,C}}{P_{th,\infty}} \right)^2 \left(\rho h + (0.5w/\sigma_o)U_a \right) + \gamma \left(\frac{P_{th,C}}{P_{th,\infty}} \right) \left(\frac{\sigma_o + 0.5w - g}{v^{0.5}} \right) w = \rho h + (0.5g/\sigma_o)U_a \quad (11)$$

This dependence of the threshold power explicitly incorporates the effect of the writing speed. The contribution due to reduced TPP goes to zero when the overlap spacing increases beyond the line width. However, the contribution due to increased single-photon absorption by the cured resist is still present as long as some portion of the adjacent line falls within the beam width. In combination, these two effects lead to a reduction in the damage threshold as the overlap spacing is varied over a wide range.

CONCLUSIONS

Herein, we have quantified the laser damage that occurs due to proximity of features. In general, the proximity effect reduces the laser damage power threshold for overlapping features. However, for physically overlapping features this decrease in threshold power does not monotonically increase with the overlap spacing. Due to this, an empirical calibration of laser damage at a select few intermediate overlap spacings does not provide a reliable estimate of the lower bound of the damage threshold. Instead, one must calibrate the damage threshold over a wider range of overlap spacing spanning from full overlap to at least a spacing of one line width. We have also identified that the proximity effect arises out of a combination of reduced two-photon polymerization and increased single photon absorption behavior of the cured resin for overlapping features. The empirical data and scaling model generated here can be used to properly select the writing parameters to prevent laser damage during printing of dense features thereby enabling high-quality additive manufacturing of millimeter scale parts with sub-micron building blocks.

ACKNOWLEDGMENTS

This work was performed under the auspices of the U.S. Department of Energy by Lawrence Livermore National Laboratory under contract DE-AC52-07NA27344. Funding was available via Laboratory Directed Research and Development project #16-ERD-006. (Document release #LLNL-CONF-679759)

S.K.S. would like to thank Dr. Chris Orme for access to and assistance with AFM imaging and Dr. James Oakdale for help with the Nanoscribe system.

REFERENCES

1. Cumpston, B.H., et al., *Two-photon polymerization initiators for three-dimensional optical data storage and microfabrication.* Nature, 1999. **398**(6722): p. 51-54.

2. Wu, S., J. Serbin, and M. Gu, *Two-photon polymerisation for three-dimensional micro-fabrication.* Journal of Photochemistry and Photobiology A: Chemistry, 2006. **181**(1): p. 1-11.

3. Farsari, M., et al., *Two-photon polymerization of an Eosin Y-sensitized acrylate composite.* Journal of Photochemistry and Photobiology A: Chemistry, 2006. **181**(1): p. 132-135.

4. Serbin, J., A. Ovsianikov, and B. Chichkov, *Fabrication of woodpile structures by two-photon polymerization and investigation of their optical properties.* Optics Express, 2004. **12**(21): p. 5221-5228.

5. Serbin, J., et al., *Femtosecond laser-induced two-photon polymerization of inorganic–organic hybrid materials for applications in photonics.* Optics Letters, 2003. **28**(5): p. 301-303.

6. So, P.T.C., *Two-photon fluorescence light microscopy*, in *Encyclopedia of Life Sciences*. 2002, Nature Publishing Group.

7. Mueller, J.B., et al., *In-situ local temperature measurement during three-dimensional direct laser writing.* Applied Physics Letters, 2013. **103**(12): p. 123107.

8. Bass, M., *HANDBOOK OF OPTICS* 2ed. Vol. 1. 1994: McGraw-Hill Professional.